Inorg. Chem. **2008**, *47*, 912–920

Reversible NO Motion in Crystalline [Fe(Porph)(1-MeIm)(NO)] Derivatives

Nathan J. Silvernail,[†] Jeffrey W. Pavlik,[†] Bruce C. Noll,[†] Charles E. Schulz,[‡] and W. Robert Scheidt*,[†]

Contribution from the Department of Chemistry and Biochemistry, University of Notre Dame, Notre Dame, Indiana 46556, and Department of Physics, Knox College, Galesburg, Illinois 61401

Received August 29, 2007

The synthesis, characterization, and X-ray structures of three low-spin (nitrosyl)iron(II) tetraarylporphyrinates, [Fe(T*p*XPP)(NO)(1-MeIm)], where X = F (in a triclinic and a monoclinic form) and OCH_3 are reported. All three molecules, at 100 K, have a single orientation of NO. These structures are the first examples of ordered NO's in [Fe(Porph)(NO)(1-MeIm)] complexes. The three new derivatives have similar structural features including a previously unnoted "bowing'' of the N_{NO}–Fe–N_{Im} angle caused by a concerted tilting of the axial Fe–N_{NO} and Fe–N_{Im} bonds. Structural features such as the displacement of Fe out of the mean porphyrin plane toward NO, tilting of the Fe–N_{NO} bond off the heme normal, and the asymmetry of the Fe–N_{por} bonds further strengthen and confirm observations from earlier studies. The [Fe(T*p*XPP)(NO)(1-MeIm)] complexes were also studied at temperatures between 125 and 350 K to investigate temperature-dependent variations and trends in the coordination group geometry. At varying temperatures (above 150 K), all three derivatives display a second orientation of the NO ligand. The population and depopulation of this second orientation are thermally driven, with no apparent hysteresis. Crystal packing appears to be the significant feature in defining the order/disorder of the NO ligand. The length of the bond trans to NO, Fe–N_{Im}, was also found to be sensitive to temperature variation. The Fe–N_{Im} bond length increases with increased temperature, whereas no other bonds change appreciably. The temperature-dependent Fe–N_{Im} bond length change and cell volume changes are consistent with a "soft" Fe–N_{Im} bond. Variable-temperature measurements show that the N–O stretching frequency changes with the Fe–N_{Im} bond length. Temperature-dependent changes in the Fe–N_{Im} bond length and N–O stretching frequency were also found to be completely reversible with no apparent hysteresis.

Introduction

Nitric oxide (NO) coordination to heme proteins has many physiological consequences. It has been implicated in a number of fundamental processes including smooth muscle relaxation,[1,2] platelet deaggregation,[3] neuronal communication,[4] aspects of myocardial function, and numerous other physiological functions.[5] NO is synthesized by nitric oxide synthase by a heme-mediated oxidation of L-arginine[6−8] or from NO_3^-/NO_2^-.[9] In many heme proteins, the NO ligand is coordinated trans to a histidine ligand.[10,11] Coordination of NO to the five-coordinate, high-spin iron(II) results in a spin transition to low spin, moves the iron center from ∼0.30−0.40 Å out-of-plane to a position in the heme plane, and causes an elongation of the Fe−His(Im) bond. Modulation of the length of this bond is thought to have important biological implications.[10−12]

* To whom correspondence should be addressed. E-mail: scheidt.1@nd.edu. Fax: (574) 631-6652.
[†] University of Notre Dame.
[‡] Knox College.

(1) Rapoport, R. M.; Murad, F. *Circ. Res.* **1983**, *52*, 352.
(2) Ignarro, L. J.; Adams, J. B.; Horwitz, P. M.; Wood, K. S. J. *Biol. Chem.* **1986**, *261*, 4997.
(3) Azuma, H.; Ishikawa, M.; Sekizaki, S. *Br. J. Pharmacol.* **1986**, *88*, 411. Furlong, B.; Henderson, A. H.; Lewis, M. J.; Smith, J. A. *Br. J. Pharmacol.* **1987**, *90*, 687. Radomski, M. W.; Palmer, R. M. J.; Moncada, S. *Br. J. Pharmacol.* **1987**, *92*, 639.
(4) Garthwaite, J. *Trends Neurosci.* **1991**, *14*, 60.
(5) Koshland, D. E., Jr. *Science* **1992**, *258*, 1861. Butler, A. R.; Williams, D. L. H. *Chem. Soc. Rev.* **1993**, *233*. Moncada, S.; Palmer, R. M. J.; Higgs, E. A. *Pharmacol. Rev.* **1991**, *43*, 109.
(6) Marletta, M. A. *J. Biol. Chem.* **1993**, *17*, 12231.
(7) Griffith, O. W.; Stuehr, D. J. *Annu. Rev. Physiol.* **1995**, *57*, 707.
(8) Alderton, W. K.; Cooper, C. E.; Knowles, R. G. *Biochem. J.* **2001**, *357*, 593. Griffith, O. W.; Stuehr, D. *J. Annu. Rev. Physiol.* **1995**, *57*, 707.
(9) Averill, B. A. *Chem. Rev.* **1996**, *96*, 2951. Eich, R. F.; Li, T.; Lemon, D. D.; Doherty, D. H.; Curry, S. R.; Aitken, J. F.; Mathews, A. J.; Johnson, K. A.; Smith, R. D.; Phillips, Jr.; Olson, G. N. *J. S. Biochemistry* **1996**, *35*, 6976.
(10) Boon, E. M.; Marletta, M. A. *J. Inorg. Biochem.* **2005**, *99*, 892.
(11) Gilles-Gonzalez, M.-A., Gonzalez, G. *J. Inorg. Biochem.* **2005**, *99*, 1.

10.1021/ic701700p CCC: $40.75
Published on Web 01/04/2008

The NO ligand imparts a strong trans effect that can cause the rupture of the Fe−His bond in a number of protein systems to give five-coordinate {FeNO}^{7} systems,[10,13,14] whereas in others, upon NO binding the heme remains a six-coordinate {FeNO}^{7} system.[13,15] This is the activation "switch'' in one example of an NO sensing protein, sGC[16] − with an apparent rupture of the Fe−His bond.[12] Structural changes induced by the elongation and eventual scission of this bond are believed to be essential in signal transduction in endothelial cells, ultimately leading to vasodilatation.[10,17]

The strength of the Fe−His(Im) bond in five-coordinate hemes has been used as a gauge of protein ligation and activation states and as a possible predictor of protein activity. The Fe−His(Im) bond strength in five-coordinate hemes is readily studied with vibrational spectroscopy.[13,18,19] Unfortunately, much less information is available about the Fe−His(Im) bond in six-coordinate iron(II) hemes with diatomic ligands that would provide information on details of, for example, control of ligand binding. Some insight into the nature of the Fe−His(Im) bond post ligand ejection has been attained through flash photolysis experiments with MbXO and HbXO.[18,20] Additional vibrational information has come from nuclear resonance vibrational spectroscopy (NRVS).[21] This experimental technique, combined with theoretical investigations, has provided significant new information on the nature of the Fe−His(Im) vibrational modes in the [Fe^{II}(Porph)(RIm)(XO)] systems.[22−24]

The power of these NRVS studies has stimulated us to further synthesize and characterize a number of new [Fe^{II}(Porph)(RIm)(XO)] complexes for such studies. In addition, this preparative and characterization work has had some interesting and unanticipated benefits. Small-molecule X-ray diffraction studies, for example, have demonstrated changes in the iron coordination chemistry between [Fe^{II}(Porph)(NO)] and [Fe^{II}(Porph)(RIm)(NO)] systems.[25] Detailed structural and vibrational correlation in ligand bonding parameters (the inverse Fe−C and C−O relationship) have been made for [Fe^{II}(Porph)(RIm)(CO)] systems.[26] In this paper, we report the synthesis and characterization of a series of [Fe^{II}(Porph)(1-MeIm)(NO)] complexes. The analyses of their molecular structures, over a range of temperatures, has provided interesting information on the nature of the motion of the axial NO ligand in the solid state. Moreover, the Fe−His(Im) interaction displays temperature-dependent behavior that can be monitored by both molecular structure determinations and variable-temperature infrared spectroscopy.

Experimental Section

General Information. All reactions were carried out under anaerobic conditions. Chloroform (Fisher), 1-propanol (Acros), and 1-methylimidazole (Acros) were used as received. Nitric oxide (Mittler Specialty Gases) was purified by passing it through a trap containing 4 Å molecular sieves immersed in an ethanol/dry ice slurry.[27] Free base porphyrins [H_2Porph] were prepared according to Adler et al.[28] [Fe(Porph)(Cl)] was prepared according to the metalation procedure of Adler et al.[29]

Synthesis of [Fe(Porph)(NO)(1-MeIm)]. The [Fe(Porph)(NO)(1-MeIm)] derivatives (Porph = T*p*FPP or T*p*OCH$_3$PP) were prepared using modifications of a previously reported synthesis.[25] Approximately 30 mg of [Fe(Porph)(Cl)] was placed into a 10 mL beaker along with 3 mL of chloroform and 3 mL of 1-methylimidazole. This beaker was then placed into a crystallization jar along with 0.5 mL of 1-propanol, 2 mL of chloroform, and 3 mL of 1-methylimidazole, then subsequently sealed with a rubber stopper. The system was purged with Ar for 10 min, and NO was bubbled through the inner and outer solutions for 10 min. High-quality crystals were obtained after 3 weeks.

X-ray Crystallographic Studies. X-ray diffraction data were collected and integrated using a Bruker x8 or D8 Apex II system, with graphite-monochromated Mo Kα (λ = 0.71073 Å) radiation from 100 to 350 K (700 Series Oxford Cryostream). The Oxford control unit is calibrated at the factory using the phase change of Rochelle's salt at 109 K.[30] The factory calibration was checked in our laboratory with an iron−constantan thermocouple and an Omega 199 temperature meter. All reported temperatures are believed accurate to within 2 K. The programs SADABS[31] and

(12) Zhao, Y.; Hoganson, C.; Babcock, G. T.; Marletta, M. A. *Biochemistry* **1998**, *37*, 12458.
(13) Schelvis, J. P. M.; Seibold, S. A.; Cerda, J. F.; Garavito, R. M.; Babcock, G. T. *J. Phys. Chem. B* **2000**, *104*, 10844.
(14) Andrew, C. R.; Kemper, L. J.; Busche, T, L.; Tiwari, A. M.; Kecskes, M. C.; Stafford, J. M.; Croft, L. C.; Lu, S.; Moënne-Loccoz, P.; Huston, W.; Moir, J. W. B.; Eady, R. R. *Biochemistry* **2005**, *44*, 8664.
(15) Ma, X.; Sayed, N.; Beuve, A.; van den Akker, F. *EMBO J.* **2007**, *26*, 578.
(16) The following abbreviations are used in this paper. sGC, soluble guanylate cyclase; NO, nitric oxide; mono, monoclinic; tri, triclinic; Porph, generalized porphyrin dianion; T*p*FPP, dianion of *meso-p*-fluorotetraphenylporphyrin; TPP, dianion of *meso*-tetraphenylporphyrin; 1-MeIm, 1-methylimidazole; R-Im, generalized substituted imidazole. Spectroscopic techniques: IR, infrared absorption spectroscopy; rR, resonance Raman spectroscopy; NRVS, nuclear resonance vibrational spectroscopy.
(17) (a) Stamler, J. S.; Feelisch, M. *In Method in Nitric Oxide Research*; Stamler, J. S., Feelisch, M., Eds.; Wiley and Sons: New York, 1996; pp 19−27. (b) Craven, P. A.; Ignarro, L. J. In *Methods in Nitric Oxide Research*; Stamler, J. S., Feelisch, M., Eds.; Wiley and Sons: New York, 1996; pp 210−220.
(18) Sage, J. T.; Champion, P. M. Small Substrate Recognition in Heme Proteins. In *Comprehensive Supramolecular Chemistry*; Suslick, K. S., Ed.; Pergamon: Oxford, UK, 1996; Vol. 5, pp 171−217.
(19) Spiro, T. G.; Li, X.-Y. Resonance Raman Spectroscopy of Metalloporphyrins. In *Biological Applications of Raman Spectroscopy*; Spiro, T. T., Ed.; John Wiley and Sons, Inc.: New York, 1988; pp 1−38.
(20) Rousseau, D. L.; Friedman, J. M. Transient and Cryogenic Studies of Photodissociated Hemoglobin and Myoglobin. In *Biological Applications of Raman Spectroscopy*; Spiro, T. G., Ed.; John Wiley and Sons, Inc.: New York, 1988; pp 133−216.
(21) Scheidt, W. R.; Durbin, S. M.; Sage, J. T. *J. Inorg. Biochem.* **2005**, *99*, 60.
(22) Rai, B. K.; Durbin, S. M.; Prohofsky, E. W.; Sage, J. T.; Ellison, M. K.; Roth, A.; Scheidt, W. R.; Sturhahn, W.; Alp, E. E. *J. Am. Chem. Soc.* **2003**, *125*, 6927.
(23) Silvernail, N. J.; Barabanschikov, A.; Pavlik, J. W.; Noll, B. C.; Zhao, J.; Alp, E. E.; Sturhahn, W.; Sage, J.T.; Scheidt, W. R. *J. Am. Chem. Soc.* **2007**, 2200.
(24) Leu, B. M.; Silvernail, N. J.; Zgierski, M. Z.; Wyllie, G. R. A.; Ellison, M. K.; Scheidt, W. R.; Zhao, J. Y.; Sturhahn, W.; Alp, E. E.; Durbin, S. M.; Sage, J. *Biophys. J.* **2007**, *92*, 3764.
(25) Wyllie, G. R. A.; Schulz, C. E.; Scheidt, W. R. *Inorg. Chem.* **2003**, *42*, 5722.
(26) Silvernail, N. J.; Roth, A.; Schulz, C. E.; Noll, B. C.; Scheidt, W. R. *J. Am. Chem. Soc.* **2005**, *127*, 14422.
(27) Dodd, R. E.; Robinson, P. L. *Experimental Inorganic Chemistry*; Elsevier: New York, 1957; p 253.
(28) Adler, A. D.; Longo, F. R.; Finarelli, J. D.; Goldmacher, J.; Assour, J.; Korsakoff, L. *J. Org. Chem.* **1967**, *32*, 476.
(29) Adler, A. D.; Longo, F. R.; Kampus, F.; Kim, J. *J. Inorg. Nucl. Chem.* **1970**, *32*, 2443.
(30) Tomaszewski, P. E. *Phase Trans.* **1992**, *38*, 127.
(31) Sheldrick, G. M. *SADABS*; Universität Göttingen: Göttingen, Germany, 2006.

TWINABS[32] were applied for absorption correction. All structures were solved using the Patterson method in XS[33] and refined using XL.[34] All atoms were found after successive full-matrix least-squares refinement cycles on F^2 and refined with anisotropic thermal parameters. Hydrogen atoms were placed at calculated geometries and allowed to ride on the position of the parent atom. Hydrogen thermal parameters were set to 1.2× the equivalent isotropic U of the parent atom and 1.5× for methyl hydrogen atoms.

Complete crystallographic details are given in the Supporting Information. Data sets were acquired at multiple temperatures for each of the six-coordinate NO complexes. Mono-[Fe(T*p*FPP)(NO)(1-MeIm)] (mono = monoclinic), at 150 and 293 K, contains a second orientation of NO oxygen which has been refined with thermal parameters equal to the first orientation.[35] Tri-[Fe(T*p*FPP)(NO)(1-MeIm)] (tri = triclinic) contains a second orientation of NO oxygen in data acquired at 200, 224, 293, and 350 K. Data were acquired on a second triclinic crystal of [Fe(T*p*FPP)(NO)(1-MeIm)] which contained two twinned components related by a 180° rotation (minor component ≈ 20%). This second example of the triclinic form also contained a second orientation of NO oxygen in data acquired at 224 and 293 K. [Fe(T*p*OCH_3PP)(NO)(1-MeIm)] contains a second orientation of NO oxygen in data acquired at 293 and 330 K. Each of the [Fe(T*p*OCH_3PP)(NO)(1-MeIm)] structures contain a disordered *p*-methoxy group modeled as two positions and modest rotational disorder of the 1-methylimidazole ligand that was left unmodeled.[36]

Infrared Measurements. Infrared spectra were taken on a Nicolet Nexus 670 FT-IR spectrometer. Selected single crystals were ground/mixed minimally with KBr (50:1) to avoid loss of 1-methylimidazole ligand. The KBr pellet was placed in a Specac variable-temperature cell with an Omega Engineering CN310 solid-state temperature controller and evacuated to a pressure of 0.1 mbar. The variable-temperature cell was then placed in the Nicolet Nexus 670 FT-IR spectrometer, and spectra were taken in both ascending and descending 20 K intervals in the range of 107−348 K.

Results

The crystal and molecular structures of three six-coordinate NO iron(II) porphyrinates have been obtained at multiple temperatures between 100 and 350 K and with several crystalline specimens. [Fe(T*p*FPP)(NO)(1-MeIm)] was found to exist as two crystalline polymorphs: a monoclinic form denoted mono-[Fe(T*p*FPP)(NO)(1-MeIm)] and a triclinic form denoted tri-[Fe(T*p*FPP)(NO)(1-MeIm)]. The [Fe(T*p*OCH_3PP)(NO)(1-MeIm)] derivative was also studied. Cell parameters and crystallographic data for 18 distinct and completed measurements are summarized in Table 1. Detailed crystallographic data are presented in Tables S1−S108.

Temperature-dependent infrared spectra were taken between 105 and 350 K for [Fe(T*p*OCH_3PP)(NO)(1-MeIm)],

Table 1. Summary of Crystallographic Data for Structure Determinations

	temp, K	*a*, Å	*b*, Å	*c*, Å	α, deg	*β*, deg	*γ*, deg	*V*, Å^3	unique data	obs data[a]	final R1	final wR2
tri-[Fe(T*p*FPP)(NO)(1-MeIm)][b,c]	100	11.4205(2)	12.1603(2)	14.3296(2)	92.789(1)	102.651(1)	99.585(1)	1907.12(5)	14,421	12,319	0.0346	0.0936
	100[d]	11.4169(2)	12.1503(3)	14.3515(3)	92.814(1)	102.6570(1)	99.557(1)	1907.91(7)	13,515	11,806	0.0397	0.1104
	150	11.4758(2)	12.2062(3)	14.3005(3)	92.786(1)	102.447(1)	99.876(1)	1919.45(7)	11,154	9193	0.0358	0.0912
	175	11.5060(3)	12.2372(3)	14.2842(3)	92.810(2)	102.330(2)	100.021(2)	1927.09(8)	9120	6338	0.0462	0.1003
	200	11.5380(2)	12.2722(2)	14.2753(3)	92.831(1)	102.195(1)	100.239(1)	1936.30(6)	11,277	8929	0.0387	0.0963
	224	11.5768(2)	12.3122(2)	14.2588(2)	92.947(1)	102.020(1)	100.430(1)	1946.58(5)	12,320	9838	0.0525	0.1025
	224[d]	11.5706(2)	12.2965(2)	14.2884(3)	92.995(1)	101.992(1)	100.375(1)	1947.53(6)	14,461	11,316	0.0461	0.1235
	293	11.6818(2)	12.4161(2)	14.2276(2)	93.391(1)	101.396(1)	101.050(1)	1975.30(5)	12,497	9838	0.0435	0.1188
	293[d]	11.6848(3)	12.4010(3)	14.2498(3)	93.513(1)	101.329(1)	100.990(1)	1977.00(8)	14,847	10,371	0.0498	0.1363
	350	11.7372(19)	12.488(2)	14.217(2)	93.801(13)	100.766(12)	101.395(12)	1995.3(6)	5417	3901	0.0452	0.1040
mono-[Fe(T*p*FPP)(NO)(1-MeIm)][e,f]	100	14.1135(4)	18.7149(6)	14.8501(4)	90	97.825(1)	90	3885.9(2)	13,516	10,958	0.0383	0.0983
	125[g]	14.1567(7)	18.7925(7)	14.8762(7)	90	97.949(3)	90	3919.6(3)	6917	4252	0.0514	0.1130
	150[g]	14.1689(4)	18.8076(5)	14.8831(5)	90	98.055(2)	90	3927.0(2)	11,991	8323	0.0463	0.1099
	293[g]	14.2767(4)	19.0568(4)	15.0121(4)	90	98.893(2)	90	4035.22(18)	8554	6445	0.0518	0.1277
[Fe(T*p*OCH_3PP)(NO)(1-MeIm)][b,c]	100	9.5017(2)	14.8654(4)	16.1086(4)	101.689(1)	101.035(1)	93.966(1)	2173.07(9)	13,061	11,271	0.0360	0.0961
	100[g]	9.4683(4)	14.8148(8)	16.0442(7)	101.768(3)	100.982(2)	93.961(3)	2149.20(17)	19,696	16,354	0.0374	0.0986
	125[g]	9.6306(2)	14.9689(3)	16.1424(4)	101.822(1)	101.384(1)	93.877(1)	2218.71(9)	16,834	12,646	0.0420	0.1122
	293[g]	9.6652(3)	14.9870(4)	16.1555(4)	101.829(1)	101.538(1)	93.835(1)	2229.93(11)	12,965	10,309	0.0411	0.1105

[a] $[I > 2\sigma(I)]$. [b] $P\bar{1}$. [c] $Z = 2$. [d] Second crystal with a twinned component. [e] $P2_1/n$. [f] $Z = 4$. [g] Second crystal.

(32) Sheldrick, G. M. *TWINABS*; Universität Göttingen: Göttingen, Germany, 2006.
(33) (a) Sheldrick, G. M. *XS*; Bruker-Nonius AXS: Madison, WI, 2001. (b) Patterson, A. L. *Phys. Rev.* **1934**, *46*, 372.
(34) Sheldrick, G. M. *XL*; Bruker-Nonius AXS: Madison, WI, 2001.
(35) Although the thermal parameters of the second orientation have been refined as equal to the first orientation, there is evidence (especially in structures above 100 K) of electron density between the first and second orientations that can not be properly modeled as two or even three atoms.
(36) Attempts were made to refine the 1-methylimidazole with two rigid bodies or a disorder model with isotropic thermal parameters with no improvement to the structure.

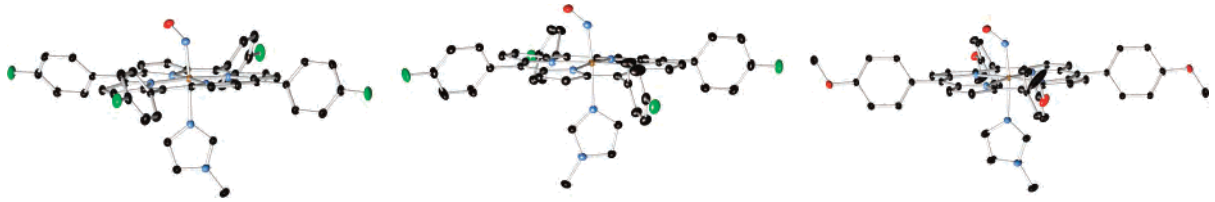

Figure 1. ORTEP diagrams (50% probability ellipsoids) of tri-[Fe(TpFPP)(NO)(1-MeIm)] (left), mono-[Fe(TpFPP)(NO)(1-MeIm)] (center), and [Fe(TpOCH$_3$PP)(NO)(1-MeIm)] (right) at 100 K. Hydrogen atoms are omitted for clarity.

Table 2. Selected Structural Features for mono-[Fe(T*p*FPP)(NO)(1-MeIm)], tri-[Fe(T*p*FPP)(NO)(1-MeIm)], [Fe(T*p*OCH$_3$PP)(NO)(1-MeIm)], and [Fe(OEP)(NO)(1-MeIm)]$^+$ at 100 K

complex	Fe−N_{NO}[a]	Fe−N_{Im}[a]	Fe−N_p[a] av	Fe−N_p[a] short	Fe−N_p[a] long	Fe−N−O[b]	Fe−N_{NO}, Fe−N_{Im} tilt[b]	N_{NO}−Fe−N_{Im}[b]	N−O[a]
tri-[Fe(T*p*FPP)(NO)(1-MeIm)]	1.7521(9)	2.1689(9)	2.011(8)	2.004(3)	2.018(3)	138.64(8)	5.1, 3.3	176.08(4)	1.1819(12)
tri-[Fe(T*p*FPP)(NO)(1-MeIm)]#2	1.7593(12)[c]	2.1669(12)	2.009(9)	2.0018(18)	2.017(3)	138.12(11)	4.7, 3.3	176.30(5)	1.1843(16)
mono-[Fe(T*p*FPP)(NO)(1-MeIm)]	1.7481(11)	2.1312(11)	2.002(14)	1.992(4)	2.011(11)	137.27(9)	7.2, 2.6	175.08(4)	1.1808(14)
[Fe(T*p*OCH$_3$PP)(NO)(1-MeIm)]	1.7486(8)	2.1659(8)	2.003(14)	1.993(11)	2.014(4)	136.17(7)	4.9, 5.7	171.73(3)	1.1856(11)
[Fe(T*p*OCH$_3$PP)(NO)(1-MeIm)]#2	1.7532(10)	2.1699(11)	2.010(14)	2.000(11)	2.020(3)	135.89(9)	5.0, 6.0	171.92(4)	1.1898(14)
[Fe(OEP)(NO)(1-MeIm)]$^{+}$[d]	1.6465(17)	1.9889(16)	2.003(5)			177.28(17)		178.75(8)	1.135(2)

[a] In Å. [b] In deg. [c] Crystal contains a twinned component. [d] At 130 K.[38]

tri-[Fe(T*p*FPP)(NO)(1-MeIm)], and mono-[Fe(T*p*FPP)(NO)-(1-MeIm)]. Experiments were performed in both ascending and descending temperature order with no indication of hysteresis.

Discussion

The structural and vibrational parameters of three complexes, [Fe(Porph)(1-MeIm)(NO)], differing only in the para substituent of the four aryl groups, display temperature-dependent variations. Moreover, the variation of these systems displays apparent reversibility with no detectable hysteresis.

Molecular Structures, 100 K. We report the crystal and molecular structures of the three iron(II) porphyrinates: tri-[Fe(T*p*FPP)(NO)(1-MeIm)],[37] mono-[Fe(T*p*FPP)(NO)(1-MeIm)], and [Fe(T*p*OCH$_3$PP)(NO)(1-MeIm)]. The molecular structures, at 100 K, are illustrated in Figure 1. The nitrosyl ligand is completely ordered in all three derivatives; these are the first examples of completely ordered nitrosyls in six-coordinate [Fe(Porph)(NO)(1-MeIm)] complexes. The three new derivatives have similar structural features. Selected geometrical parameters are given in Table 2. For comparison, the only example of the related iron(III) derivative[38] is also given in the table. Two independent determinations of structure at 100 K were carried out for tri-[Fe(T*p*FPP)(NO)-(1-MeIm)] and [Fe(T*p*OCH$_3$PP)(NO)(1-MeIm)]; the averaged values for the two determinations will be cited. The observed values for the Fe−N_{NO} bond distance, the N−O bond distance, and the Fe−N−O bond angle are all similar. Values for tri-[Fe(T*p*FPP)(NO)(1-MeIm)], mono-[Fe(T*p*FPP)(NO)(1-MeIm)], and [Fe(T*p*OCH$_3$PP)(NO)(1-MeIm)], respectively, are 1.7481(11), 1.756(5) (av), and 1.751(3) (av) Å for the Fe−N_{NO} bond distance; 1.1808(14), 1.183(2) (av), and 1.188(3) (av) Å for the N−O bond distance; and 137.27-(9)°, 138.4(4)° (av), and 136.0(2)° (av) for the Fe−N−O bond angle.

Several additional features of six-coordinate {FeNO}^{7} porphyrinates are summarized in the formal core diagrams given in Figure 2. One feature is the displacement of the Fe from the 24-atom mean plane. In all cases there is a small (0.05−0.08 Å) displacement toward the NO ligand. The projection of the Fe−N_{NO} vector onto the porphyrin plane is displayed in Figure 2 as the short line; the small circle represents the oxygen position. The projection of the imidazole onto the porphyrin plane is displayed in Figure 2 as the long line; the large circle represents the position of the 1-methyl group. The projection of Fe−N_{NO} is close to bisecting a pair of Fe−N_p bonds; the actual values and the angle between the FeNO and imidazole planes are also shown in the figure.

As can be seen in Figure 1, the Fe−N_{NO} vector is tilted off-axis from the heme normal in the direction of the NO oxygen atom. The tilts for mono-[Fe(T*p*FPP)(NO)(1-MeIm)], tri-[Fe(T*p*FPP)(NO)(1-MeIm)], and [Fe(T*p*OCH$_3$PP)(NO)-(1-MeIm)] are 7.1°, 4.8(3)° (av), and 5.0(1)° (av), respectively. This tilt appears to be a direct effect of the FeNO bonding; we find no steric reasons for the tilts. Moreover, this tilt is associated with an asymmetry in the equatorial Fe−N_p bonds. The two Fe−N_p bonds that bracket the NO ligand are shorter than the average, whereas the other two are longer. This asymmetry is clearly a bonding effect. Porphyrin core asymmetry is also observed in five-coordinate {FeNO}^{7} porphyrinates.[39] For the complexes mono-[Fe-(T*p*FPP)(NO)(1-MeIm)], tri-[Fe(T*p*FPP)(NO)(1-MeIm)], and [Fe(T*p*OCH$_3$PP)(NO)(1-MeIm)], respectively, the two short Fe−N_p bonds are 1.992(4), 2.003(2) (av), and 1.996(10) Å (av), while the long Fe−N_p bonds are: 2.011(11), 2.017(3) (av), and 2.017(5) Å (av), respectively. Since the first experimental elaboration of the tilt and equatorial asymmetry,

(37) An analysis of the NRVS vibrational spectra of tri-[Fe(T*p*FPP)(NO)-(1-MeIm)] and mono-[Fe(T*p*FPP)(NO)(1-MeIm)] and the 100 K structures have been previously reported.[23]

(38) Ellison, M. K.; Scheidt, W. R. *J. Am. Chem. Soc*. **1999**, *121*, 5210.

(39) Ellison, M. K.; Scheidt, W. R. *J. Am. Chem. Soc*. **1997**, *119*, 7404.

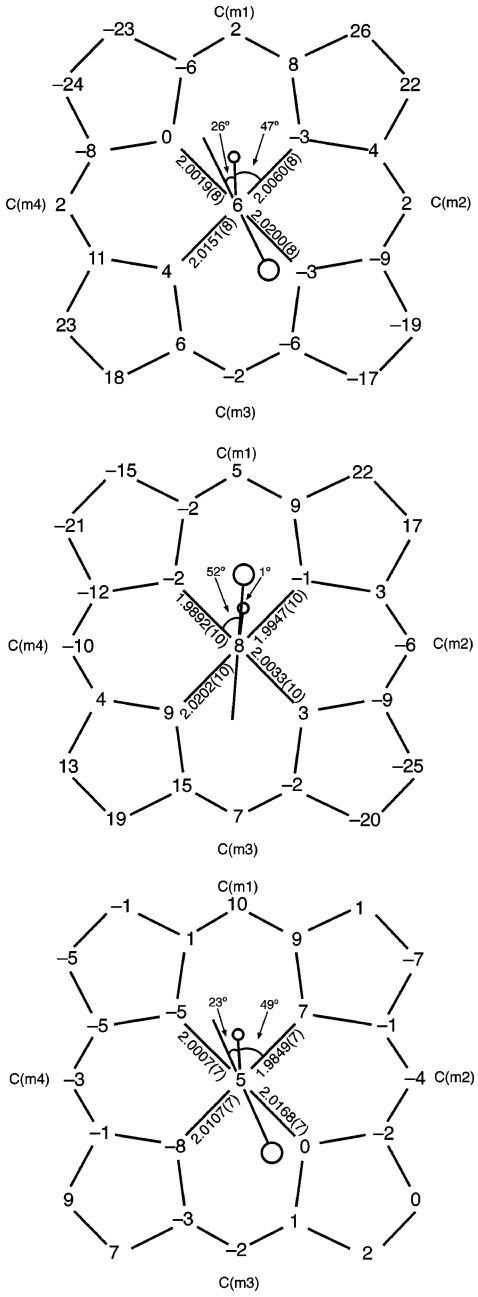

Figure 2. Formal diagram of the porphyrinato core of tri-[Fe(TpFPP)(1-MeIm)(NO)] (top), mono-[Fe(TpFPP)(1-MeIm)(NO)] (middle), and [Fe(TpOCH$_3$PP)(NO)(1-MeIm)] (bottom) at 100 K displaying the perpendicular displacements (in units of 0.01 Å) of the core atoms from the 24-atom mean plane. Positive displacements are toward the nitrosyl-coordinated face, while the imidazole ligand is displaced on the negative side of the porphyrin core. The orientation of the imidazole ligand with respect to the porphyrin core is also illustrated. The location of the 1-methyl group is represented by the large circle, while the location of the nitrosyl projection onto the porphyrin core is indicated by the small circle. Fe−Np bond distances (Å) and angles (deg) are also displayed.

a number of DFT calculations[40−44] have provided an electronic basis for ligand-based asymmetry.

The Fe−N_{Im} bond is also tilted off-axis, but by smaller amounts. Moreover, as can be seen in Figure 1, the imidazole tilt and the NO tilt are toward each other so as to lead to a "bowing'' in the N_{NO}−Fe−N_{Im} bond angle. "Bowing'' of the N_{NO}−Fe−N_{Im} unit is not unique to these porphyrinates. Although it has not been noted previously, this feature is

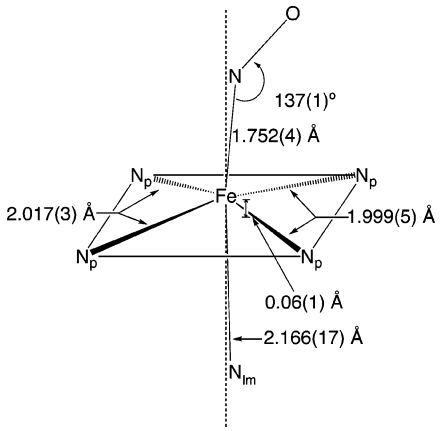

Figure 3. Selected structural features of [Fe(Porph)(1-MeIm)(NO)] with standard deviations. Standard deviations are based on the five 100 K structures presented herein and two previous structure determinations[25,40] and the assumption that all are drawn from the same population.

general to all six-coordinate {FeNO}^{7} porphyrinates; it is also observed in [Fe(TPP)(NO)(1-MeIm)],[25,45] [Fe(TPP)(NO)(4-NMe$_2$Py)],[25] and [Fe(T*o*F$_2$PP)(NO)(1-MeIm)].[40]

A saddling pattern is observed for the core 24 atoms of tri-[Fe(T*p*FPP)(NO)(1-MeIm)] and mono-[Fe(T*p*FPP)(NO)(1-MeIm)], while in [Fe(T*p*OCH$_3$PP)(NO)(1-MeIm)] the core is only modestly ruffled. Saddling is a commonly observed core conformation of six-coordinate iron(II) porphyrinates with a single axial diatomic ligand. Saddled cores have been observed in [Fe(TPP)(NO)(1-MeIm)],[25] [Fe(TPP)(NO)(4-NMe$_2$Py)],[25] and [Fe(TPP)(NO)(4-MePip)].[25]

The structures of these three six-coordinate {FeNO}^{7} porphyrinates further strengthen and confirm observations made during earlier studies.[25,40,45] Wyllie et al. suggested a best set of structural parameters for six-coordinate {FeNO}^{7} porphyrinates.[25] With the inclusion of the additional points presented herein, the canonical values for the bonding parameters of six-coordinate {FeNO}^{7} porphyrinates with imidazole ligation may now be even more firmly assigned. Selected average structural parameters and standard deviations[46] for [Fe(Porph)(NO)(1-MeIm)] are given in Figure 3. Data include the five 100 K structures presented herein and two previous structure determinations.[25,40] The range of bond lengths for each of the bonding parameters is small, with the exception of the Fe−N_{Im} bond, which is known to be very long, owing to the structural trans effect of NO. The average values of bonding parameters agree well with those presented previously as general parameters for six-coordinate {FeNO}^{7} porphyrinates[25] yet give additional information due to the multiple data collections and the high precision of the data.

(40) Praneeth, V. K. K.; Näther, C.; Peters, G.; Lehnert, N. *Inorg. Chem.* **2006**, *45*, 2795.
(41) Cheng, L.; Novozhilova, I.; Kim, C.; Kovalevsky, A.; Bagley, K. A.; Coppens, P. Richter-Addo, G. B. *J. Am. Chem. Soc.* **2000**, *122*, 7142.
(42) Ghosh, A.; Wondimagegn, T. *J. Am. Chem. Soc.* **2000**, *122*, 8101. Ghosh, A. *Acc. Chem. Res.* **2005**, *38*, 943.
(43) Rovira, C.; Kunc, K.; Hutter, J.; Ballone, P.; Parrinello, M. *J. Phys. Chem. A* **1997**, *101*, 8914.
(44) Patchkovskii, S.; Ziegler, T. *Inorg. Chem.* **2000**, *39*, 5354.
(45) Scheidt, W. R.: Piciulo, P. L. *J. Am. Chem. Soc.* **1976**, *98*, 1913.
(46) Standard deviations are calculated on the assumption that the values are taken from the same population.

Molecular Structures, Multiple Temperatures. A "fortuitous'' failure of the crystal cooling system led to the collection of a data set for tri-[Fe(T*p*FPP)(NO)(1-MeIm)] at room temperature. The structure revealed two orientations of the NO ligand; a disordered NO is common with many prior examples.[25,40,45,47] Upon repair of the cryocooler, the structure was redetermined at 100 K. The same crystalline sample now showed a single orientation of the NO ligand at the lower temperature. This suggests that the second orientation of NO in tri-[Fe(T*p*FPP)(NO)(1-MeIm)] is a temperature-dependent phenomenon. Accordingly, we collected a number of additional data sets at different temperatures and on two crystal samples for tri-[Fe(T*p*FPP)(NO)(1-MeIm)].[48,49] A total of 10 distinct data sets were collected; the order of data collections is indicated in Table 3. The graphical depiction in Figure 4 shows experiment order, experiment temperature, NO orientations, and the population of the major NO orientation. Several generalizations are apparent from the figure for tri-[Fe(T*p*FPP)(NO)(1-MeIm)]. First, at low temperature the NO ligand is ordered for two different crystal samples. Second, similar populations of the NO orientation are observed at the same temperature. Third, the population of the second orientation increases with increasing temperature. Fourth, the order/disorder of NO is a thermally driven, reversible process. Finally, the results appear to be sample independent, although in this experiment and the others following have been necessarily limited to two samples each.

A smaller set of temperature-dependent structure determinations were subsequently made for mono-[Fe(T*p*FPP)-(NO)(1-MeIm)] and [Fe(T*p*OCH_3PP)(NO)(1-MeIm)].[50] Again, temperature-dependent NO orientational disorder was observed. The experimental order given in Table 3 also shows apparent reversibility of the NO orientation. At room temperature, two orientations of NO were found in both complexes. However, at lower temperatures, each of the two samples contains only a single orientation of the NO ligand.

These three studies allow for the observation of possible temperature-dependent variations or trends in the coordination group geometry of {FeNO}^{7} porphyrinates. Bond lengths, angles, and other geometrical parameters for the coordination group are given in Table 3. The metrical parameters show little or no temperature dependence. Although a second orientation of the NO becomes evident at higher temperatures, the absolute and relative orientations of the imidazole and the major NO orientation do not show any temperature dependence. Formal core diagrams of all derivatives at all measured temperatures are given in Figures S1−S3, which show this invariance, as well as only very small differences in core conformations. The Fe−N_{Im}

Table 3. Selected Structural Features and Nitrosyl Stretching Frequencies for mono-[Fe(T*p*FPP)(NO)(1-MeIm)] and tri-[Fe(T*p*FPP)(NO)(1-MeIm)]

complex	temp,[a] [expt order]	Fe−N_{NO}[b]	Fe−N_{Im}[b]	Fe−N_p[b]	Fe−N_p[b] short	Fe−N_p[b] long	Fe−N−O[c]	Fe−N_{NO}, Fe−N_{Im} tilt[c,d]	N_{NO}−Fe−N_{Im}[c]	N−O[b]	ν_{N-O}[e]	rotation change[c,f]	% maj orien
tri-[Fe(T*p*FPP)-(NO)(1-MeIm)][g]	100 [4]	1.7521(9)	2.1689(9)	2.011(8)	2.004(3)	2.018(3)	138.64(8)	5.1, 3.3	176.08(4)	1.1819(12)	1635.74	206	100
	100 [3]	1.7593(12)	2.1669(12)	2.009(9)	2.0018(18)	2.017(3)	138.12(11)	4.7, 3.3	176.30(5)	1.1843(16)	1635.74	206	100
	150 [7]	1.7480(12)	2.1725(12)	2.007(8)	2.0021(12)	2.015(5)	138.89(11)	4.6, 2.8	176.10(5)	1.1807(15)	1636.73	205	100
	175 [8]	1.743(2)	2.1724(19)	2.007(10)	2.0010	2.017(6)	138.90(16)	4.6, 2.7	176.38(8)	1.182(3)	1637.23	206	100
	200 [9]	1.7477(13)	2.1774(13)	2.008(9)	2.002(2)	2.016(4)	138.99(12)	4.6, 3.0	176.33(5)	1.1788(17)	1637.72	207, 27	96
	224 [6]	1.7473(12)	2.1814(12)	2.008(6)	2.0030(6)	2.014(2)	138.95(12)	4.3, 2.8	176.50(5)	1.1798(17)	1638.20	207, 28	94
	224 [2]	1.7579(14)	2.1880(14)	2.009(7)	2.0038(4)	2.015(2)	138.13(15)	3.9, 5.5	176.76(6)	1.182(2)	1638.20	207, 28	93
	293 [5]	1.7427(14)	2.1906(14)	2.007(5)	2.004(2)	2.012(3)	138.77(16)	3.4, 2.5	177.38(6)	1.188(2)	1639.56	209, 30	84
	293 [1]	1.7524(15)	2.1885(15)	2.008(5)	2.004(2)	2.012(3)	138.32(18)	3.3, 2.9	177.61(6)	1.184(2)	1639.56	209, 30	82
	350 [10][h]	1.724(3)	2.193(3)	2.006(3)	2.004(3)	2.007(3)	139.1(3)	3.2, 2.7	178.04(12)	1.194(6)	1640.69	210, 30	73
mono-[Fe(T*p*FPP)-(NO)(1-MeIm)][i]	100 [1]	1.7481(11)	2.1312(11)	2.002(14)	1.992(4)	2.011(11)	137.27(9)	7.2, 2.6	175.08(4)	1.1808(14)	1624.39	1	100
	125 [4]	1.748(3)	2.128(3)	2.003(14)	1.99(2)	2.014(11)	135.7(3)	6.1, 2.5	175.91(12)	1.215(3)	1625.18	0	100
	150 [3]	1.7558(15)	2.1325(14)	2.002(14)	1.991(6)	2.012(13)	136.54(14)	6.3, 1.9	175.71(7)	1.201(2)	1625.97	0, 84	92
	293 [2]	1.753(3)	2.158(2)	2.003(12)	1.995(1)	2.011(13)	138.2(3)	5.4, 1.7	176.54(10)	1.200(4)	1630.49	1, 79	74
[Fe(T*p*OCH_3PP)-(NO)(1-MeIm)][i]	100 [1]	1.7486(8)	2.1659(8)	2.003(14)	1.993(11)	2.014(4)	136.17(7)	4.9, 5.7	171.73(3)	1.1856(11)	1616.14	203	100
	100 [4]	1.7532(10)	2.1699(11)	2.010(14)	2.000(11)	2.020(3)	135.89(9)	5.0, 6.0	171.92(4)	1.1898(14)	1616.14	203	100
	293 [2]	1.7464(12)	2.1992(12)	2.009(12)	2.000(8)	2.018(5)	135.83(12)	4.6, 6.0	173.10(5)	1.2004(20)	1619.53	201, 286	80
	330 [3]	1.7438(14)	2.2030(14)	2.008(10)	1.999(7)	2.016(4)	135.88(15)	4.1, 5.7	173.39(6)	1.210(2)	1620.18	202, 287	76

[a] In K. [b] In Å. [c] In deg. [d] Uncertainties at 100 K are about 0.1° and are somewhat larger at higher temperatures where disordered NO is found, see text. [e] In cm^{-1}. Frequencies for a particular temperature are interpolated from the best fit line in Figure 7. [f] 0° is the 1-methyl group position of 1-MeIm, rotations are clockwise. [g] Experiments 1−3 used a crystal with a twin component. Experiments 4−10 used a second crystal with no twinning. [h] See ref 49. [i] Experiments 2−4 used a second crystal.

(47) Scheidt, W. R.; Brinegar, A. C.; Ferro, E. B.; Kirner, J. F. *J. Am. Chem. Soc.* **1977**, *99*, 7315.

(48) ORTEP diagrams of tri-[Fe(T*p*FPP)(NO)(1-MeIm)] at each reported temperature (see Table 3) are displayed in the Supporting Information.

(49) During the 350 K data collection for tri-[Fe(T*p*FPP)(NO)(1-MeIm)], sample decay became evident. The reported structure is based on a subset of the total reflections that represent 100% completeness to a resolution of 0.90 Å.

(50) ORTEP diagrams of mono-[Fe(T*p*FPP)(NO)(1-MeIm)] and [Fe-(T*p*OCH_3PP)(NO)(1-MeIm)] at each reported temperature (see Table 3) are displayed in the Supporting Information.

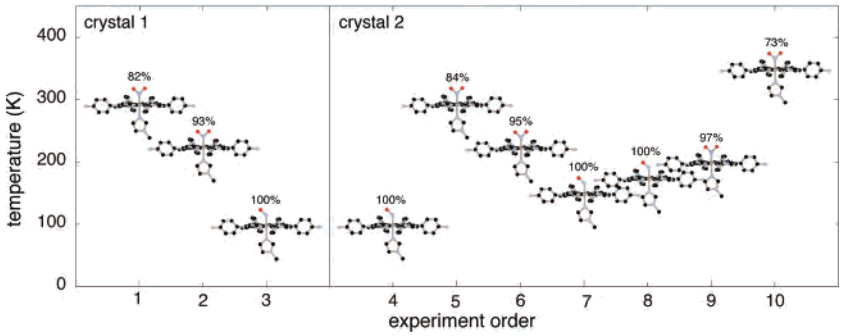

Figure 4. Diagram displaying the order of data acquisition for tri-[Fe(T*p*FPP)(NO)(1-MeIm)]. The temperature of data acquisition and occupancy factors for the major orientations are also displayed.

distance and the Fe−N_{NO} tilt angle show the largest temperature-dependent effect.

Tilting of the Fe−N_{NO} vector, as described above, is an inherent characteristic of {FeNO}^{7} porphyrinates. The Fe−N_{NO} tilt shows an apparent temperature dependence; the tilt is smaller with increased temperature. However, the true degree of temperature variation is difficult to measure due to uncertainties associated with the NO nitrogen position. The two orientations of the NO ligand lead to two positions of the nitrogen that should lead to a small change in the apparent refined position which is the average of the population-weighted positions. This, along with possible effects of increased thermal motion, leads to apparent shifts in the nitrogen position and concomitant decreases in the tilt angle that overstate the temperature-dependent change.

As displayed in Figure 3, the tilting of the Fe−N_{NO} vector in {FeNO}^{7} porphyrinates induces asymmetry in the Fe−N_p bonds. All of the complexes presented, at every temperature, have a similar pattern of a pair of shortened Fe−N_p bonds and a pair of elongated Fe−N_p bonds. Average values of short and long Fe−N_p for tri-[Fe(T*p*FPP)(NO)(1-MeIm)], mono-[Fe(T*p*FPP)(NO)(1-MeIm)], and [Fe(T*p*OCH_3PP)-(NO)(1-MeIm)], which contain a single ordered NO at 100 K, have been calculated and are displayed in Table 3. Although variation of the Fe−N_p bond lengths attributed to multiple orientations should be observed, the measured differences are smaller than the uncertainties; bond asymmetry is observed in all cases.

The strong trans effect of NO causes the rupture of the Fe−His bond in a number of protein systems to give five-coordinate {FeNO}^{7} systems,[10,13,14] while in others, upon NO binding the heme remains six-coordinate {FeNO}^{7}.[13,15] Clearly, understanding the nature of this bond and its effects are essential to understanding heme {FeNO}^{7} NO-sensing systems. The activation "switch'' in sGC is an apparent rupture of the Fe−His bond.[12] Structural changes induced by the elongation and eventual scission of this bond are believed to be essential in signal transduction, ultimately leading to vasodilatation.[10,17]

The known trans-directing effect of NO on the Fe−N_{Im} bond suggests that the bond might be described as "soft'' and be especially susceptible to temperature-dependent environmental effects.[51] This is indeed the case. The length of the biologically important Fe−N_{Im} bond in each of the three six-coordinate {FeNO}^{7} porphyrinates shows a linear

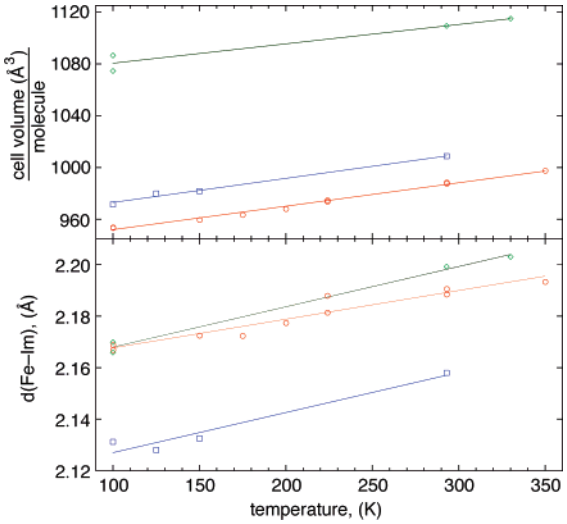

Figure 5. Plot of cell volume per molecule (Å^3) or Fe−N_{Im} bond distance (Å) vs temperature (K). Data illustrated are (red circles) tri-[Fe(T*p*FPP)-(NO)(1-MeIm)], (blue squares) mono-[Fe(T*p*FPP)(NO)(1-MeIm)], and (green diamonds) [Fe(T*p*OCH_3PP)(NO)(1-MeIm)]. Data points in each of the plots are fit linearly. Correlation coeffcients for the top[bottom] plots are tri-[Fe(T*p*FPP)(NO)(1-MeIm)] 0.99[0.96], mono-[Fe(T*p*FPP)(NO)(1-MeIm)] 0.99[0.97], and [Fe(T*p*OCH_3PP)(NO)(1-MeIm)] 0.97[0.99].[53]

dependence on temperature. Plotted in the lower panel of Figure 5 is the temperature dependence of the Fe−N_{Im} bond for tri-[Fe(T*p*FPP)(NO)(1-MeIm)], mono-[Fe(T*p*FPP)(NO)-(1-MeIm)], and [Fe(T*p*OCH_3PP)(NO)(1-MeIm)]. The change in cell volume as a function of temperature is shown in the top panel of Figure 5; the correlation between changes in cell volume and the Fe−N $_{Im}$ bond length are evident. The change in cell volumes for the three complexes between 100 and 293 K is about 3.6−3.8%. The changes in cell volume are not unusual for porphyrin complexes in our experience, although perhaps at the upper end of ranges observed.[52] The change of the Fe−N_{Im} bond distance in [Fe(T*p*OCH_3PP)-(NO)(1-MeIm)] (2.1659(8)−2.2030(14) Å, 100−330 K), tri-

(51) The binding constants for the addition of an imidazole to a five-coordinate nitrosyl are known to be small and are summarized in ref 40. Neither the trans effect or the binding constant absolutely predict that the Fe−N_{Im} bond will show a strong temperature dependence.

(52) For example, a six-coordinate CO complex showed a 3.2% change in cell volume. N. Silvernail, B. C. Noll, and W. R. Scheidt, work in progress.

(53) A linear correlation coefficient, Pearson's R,[54] was used to judge the fit to the data. $R = \sum_i (x_i - \bar{x})(y_i - \bar{y}) / \sqrt{\sum_i (x_i - \bar{x})^2} \sqrt{\sum_i (y_i - \bar{y})^2}$

(54) Walpole, R.E.; Meyers, R. H.; Meyers, S. L.; Ye, K. *Probability and Statistics for Engineers and Scientists*, 7th ed.; Prentice Hall: Upper Saddle River, NJ, 2002; pp 391−394.

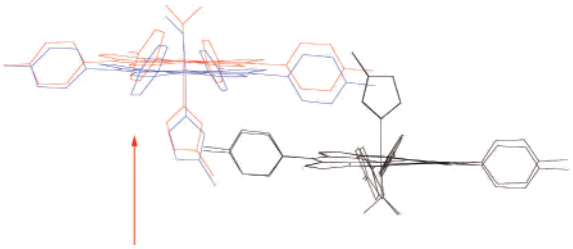

Figure 6. Overlay diagram displaying the relative shift of adjacent molecules in the unit cell for tri-[Fe(T*p*FPP)(NO)(1-MeIm)] at 100 K. The coordinates of the porphyrin nitrogen atoms of the 100 and 350 K structures have been overlaid for the two molecules shown at the bottom right. The relative differences in the intermolecular spacing of ~0.5 Å can now be seen between the 100 K structure (shown in blue) and the 350 K structure (shown in red).

[Fe(T*p*FPP)(NO)(1-MeIm)] (2.1669(12)−2.1934(28) Å, 100−350 K), and mono-[Fe(T*p*FPP)(NO)(1-MeIm)] (2.1312(11)−2.158(2) Å, 100−293 K) is small but unidirectional.

The effects of the temperature-dependent crystal packing on the Fe−N_{Im} is best seen in tri-[Fe(T*p*FPP)(NO)(1-MeIm)]. Figure 6 displays the relative shift of adjacent molecules in the unit cell for tri-[Fe(T*p*FPP)(NO)(1-MeIm)] at 100 K. In this figure, coordinates of the porphyrin nitrogen atoms of the 100 and 350 K structures have been overlaid for the two molecules shown at the bottom right. The relative differences in the intermolecular spacing of ~0.5 Å can now be seen between the 100 K structure (shown in blue) and the 350 K structure (shown in red). The contraction of the cell and the tighter intermolecular contacts in the 100 K structure can be clearly seen. This cell contraction is manifested in a shortening of Fe−N_{Im} by about 0.02 Å. Clearly, the weakness of the Fe−N_{Im} bond has contributed to the temperature dependence of the Fe−N_{Im} bond distance. The red vector shown in Figure 6 has approximately equal components in the *a* and *b* directions that are also seen in the relative changes in the cell constants. Although the directions are not as clear in [Fe(T*p*OCH_3PP)(NO)(1-MeIm)] and mono-[Fe(T*p*FPP)(NO)(1-MeIm)], they similarly display a shortening of the Fe−N_{Im} bond due to contraction of the unit cell and decreased intermolecular interactions with reduced temperature.

Variable-Temperature Infrared Studies. Temperature-dependent infrared data were collected for [Fe(T*p*OCH_3PP)-(NO)(1-MeIm)], tri-[Fe(T*p*FPP)(NO)(1-MeIm)], and mono-[Fe(T*p*FPP)(NO)(1-MeIm)] at temperatures ranging from 107 to 348 K. Infrared measurements were made to determine if the distinct NO orientations observed in the X-ray diffraction experiments would be vibrationally observable. In all three complexes, a single ν_{N-O} band was observed with no discernible broadening that might suggest a second ν_{N-O} peak. The most significant change observed was an increasing value of ν_{N-O} with increasing temperature. The temperature dependence (20 K intervals) of ν_{N-O} vs *T* is given in Figure 7. In all cases, the change in ν_{N-O} vs temperature demonstrates a linear dependence with high correlation.

What effect leads to the temperature dependence? A theoretical study of the two polymorphic forms of [Fe-(T*p*FPP)(NO)(1-MeIm)] suggested equivalent energy-minimized structures and vibrational data despite the differences

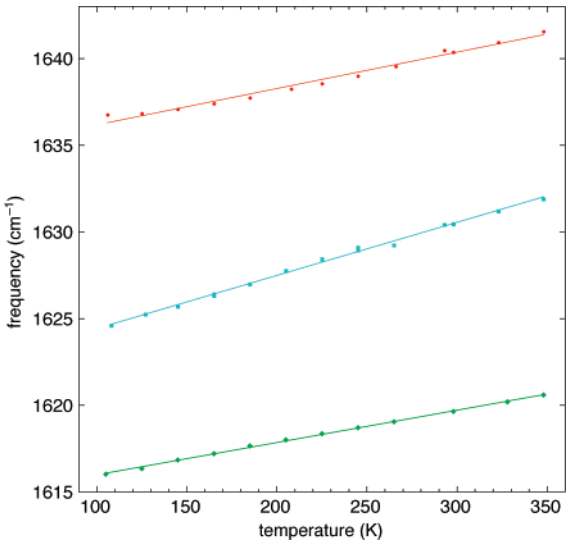

Figure 7. Plot of ν_{N-O} (cm^{-1}) vs temperature (K). Data illustrated are tri-[Fe(T*p*FPP)(NO)(1-MeIm)] (red circles), mono-[Fe(T*p*FPP)(NO)(1-MeIm)] (blue squares), and [Fe(T*p*OCH_3PP)(NO)(1-MeIm)] (green diamonds). Each set of data points is fit linearly with correlation coeffcients of $R > 0.99$.[53]

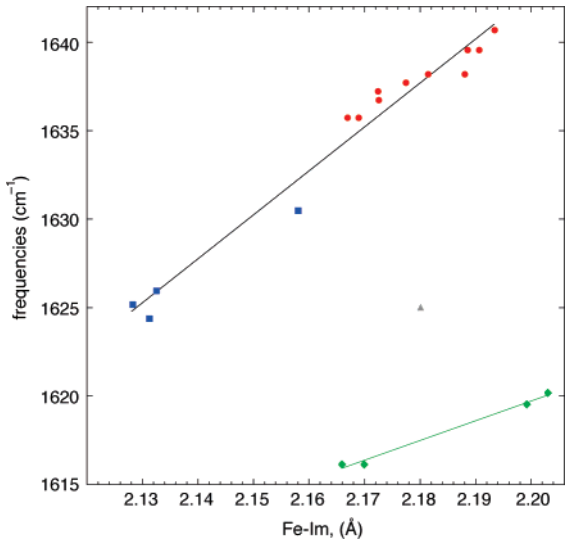

Figure 8. Plot of ν_{N-O} (cm^{-1}) vs Fe{NIm bond distance (Å). Data illustrated are triclinic (red circles) and monoclinic (blue squares) forms of [Fe(T*p*FPP)(NO)(1-MeIm)], [Fe(T*p*OCH_3PP)(NO)(1-MeIm)] (green diamonds), and [Fe(TPP)(NO)(1-MeIm)][45] (gray triangle). Frequencies for a particular temperature are interpolated from the best fit line in Figure 7. Data points are fit with a correlation coeffcient of $R = 0.98$ for [Fe(T*p*FPP)-(NO)(1-MeIm)] (black line) and $R = 0.98$ for [Fe(T*p*OCH_3PP)(NO)(1-MeIm)] (green line).[53]

in the relative orientation of the NO and imidazole planes (i.e., cisoid and transoid).[23] Thus, relative differing orientations appear not to have an effect on ν_{N-O}. Rather, we believe that it is the temperature-dependent changes in the Fe−N_{Im} bond length, not any environmental differences of the NO ligand, that causes the variation of ν_{N-O} with temperature. These values are strongly correlated for each complex. Figure 8 displays a plot of the Fe−N_{Im} bond length vs the N−O stretching frequency for tri-[Fe(T*p*FPP)(NO)(1-MeIm)] (red circles), mono-[Fe(T*p*FPP)(NO)(1-MeIm)] (blue squares), and [Fe(T*p*OCH_3PP)(NO)(1-MeIm)] (green diamonds). The two polymorphic forms of [Fe(T*p*FPP)(NO)(1-MeIm)] fall

Table 4. Mössbauer Data for Six-Coordinate [Fe(Porph)(1-MeIm)(NO)]

complex	T, K	ΔE_q, mm s^{-1}	δ, mm s^{-1}	ref
tri-[Fe(T*p*FPP)(1-MeIm)(NO)]	293	0.76	0.26	tw
	250	0.75	0.29	tw
	200	0.76	0.30	tw
	150	0.76	0.32	tw
	100	0.75	0.33	tw
	20	0.74	0.34	tw
mono-[Fe(T*p*FPP)(1-MeIm)(NO)]	293	0.75	0.22	tw
[Fe(T*p*OCH$_3$PP)(1-MeIm)(NO)]	293	0.87	0.24	tw
	200	0.86	0.29	tw
	100	0.84	0.32	tw
	20	0.83	0.33	tw
[Fe(TPP)(1-MeIm)(NO)]	293	0.80	0.24	26
	150	0.75	0.31	26
	50	0.75	0.33	26
	4.2	0.73	0.35	26

on the same line (best fit line in black) and demonstrate that the correlation is independent of crystalline form. Plots of Fe−N_{Im} vs ν_{N-O} for [Fe(T*p*OCH$_3$PP)(NO)(1-MeIm)] (green diamonds), however, do not fall onto the same line as tri-[Fe(T*p*FPP)(NO)(1-MeIm)] and mono-[Fe(T*p*FPP)(NO)(1-MeIm)]. These differences can be attributed to the cis effect of different para-substituted porphyrinates.[55] The electron-donating character of the methoxy substituent in [Fe(T*p*OCH$_3$PP)(NO)(1-MeIm)] increases the electron density on iron, thereby pushing more electron density into the SOMO and increasing the π^* antibonding character of NO. This is seen experimentally in the lower ν_{N-O} frequencies observed for [Fe(T*p*OCH$_3$PP)(NO)(1-MeIm)]. The electron-withdrawing fluoro-substituted analogue reduces electron density at the iron center, thereby causing the higher observed value for ν_{N-O} in the [Fe(T*p*FPP)(NO)(1-MeIm)] derivatives. Although a complete temperature profile for [Fe(TPP)(1-MeIm)(NO)] is not available, the room-temperature value for the parent species is in fact at an intermediate value (ν_{N-O} = 1625 cm^{-1}),[45] consistent with its expected cis effect.

Additionally, the effect of varying the length of the Fe−N_{Im} bond is different for the two porphyrinates. As observed in Figure 8, the slope of [Fe(T*p*FPP)(NO)(1-MeIm)] is more than 2× larger than in [Fe(T*p*OCH$_3$PP)(NO)(1-MeIm)]; the effect of changing the Fe−N_{Im} bond distance on ν_{N-O} is twice as large. This further reflects differences in the electronic characteristics imparted by the differing porphyrinates.

The trans effect of the heme axial ligands are thought to be of great utility to diatomic sensing heme proteins.[17] Correlations of bonding parameters across the porphyrin plane have been previously noted.[23,47] The interaction between the axial ligands in heme nitrosyls are made through the SOMO. The SOMO of [Fe(Porph)(NO)(1-MeIm)] has been described as a combination of the π^* orbital on NO and the d_{z^2} orbital and which is an antibonding interaction with respect to the imidazole ligand.[40] A shortening in the Fe−N_{Im} bond distance must lead to (small) increases in electron donation to Fe, which decreases the donation from the π^* orbital of NO and a concomitant decrease in ν(NO). The converse is also possible. There have been suggestions that distal pocket interactions, steric, electronic, or both, directly influence the proximal coordination and by association signal transduction.[15] The observation of spin−spin coupling between the imidazole ^{14}N and NO observable in the EPR spectrum of [Fe(Porph)(NO)(1-MeIm)] suggests at least modest interaction between the two axial ligands.[56]

Mössbauer spectra have been measured in a 500 mT field and at several temperatures. Values are given in Table 4. The values observed are similar to those observed previously for [Fe(TPP)(1-MeIm)(NO)][25] and are otherwise unremarkable.

Summary. Three new six-coordinate iron(II) nitrosyl-ligated porphyrinates have been prepared and characterized. At 100 K, all structures showed an ordered nitrosyl ligand and are the first examples of completely ordered nitrosyls in [Fe(Porph)(NO)(1-MeIm)] complexes. The NO ligand is disordered at higher temperatures; this change is a reversible process. The new derivatives have similar structural features including a previously unnoted "bowing'' of N_{NO}−Fe−N_{Im} caused by the concerted tilting of Fe−N_{NO} and Fe−N_{Im} bonds. The structures of these three six-coordinate {FeNO}^{7} porphyrinates further strengthen and confirm observations made during earlier studies. X-ray diffraction experiments performed at temperatures above 100 K allowed the observation of temperature-dependent variations or trends in the coordination group geometry. These trends indicate a strong correlation between the physiologically relevant Fe−N_{Im} bond and the stretching frequency of NO on the opposite side of the porphyrin.

Acknowledgment. We thank the National Institutes of Health for support of this research under Grant No. GM-38401 (W.R.S). We thank the NSF for X-ray instrumentation support through Grant No. CHE-0443233.

Supporting Information Available: Figures S1−S3, formal diagrams displaying the perpendicular displacement of core atoms from the 24-atom mean planes at all measured temperatures; Figures S4−S7, ORTEP diagrams of complexes at all temperatures; Tables S1−S108, detailed crystallographic data; crystallographic data in CIF format. This material is available free of charge via the Internet at http://pubs.acs.org.

IC701700P

(55) Buchler, J. W.; Kokisch, W.; Smith, P. D. *Struct. Bonding (Berlin)* **1978**, *34*, 79.

(56) (a) Wayland, B. B.; Olson, L. W. *J. Am. Chem. Soc.* **1974**, *96*, 6037. (b) Morse, R. H.; Chan, S. I. *J. Biol. Chem.* **1980**, *255*, 7876.